Pathways to 1.5 and 2 °C warming based on observational and geological constraints

Philip Goodwin[1], Anna Katavouta[2], Vassil M. Roussenov[2], Gavin L. Foster[1], Eelco J. Rohling[3,1] and Richard G. Williams[2]

1. Ocean and Earth Science, National Oceanography Centre Southampton, University of Southampton, Southampton, UK.
2. Department of Earth, Ocean & Ecological Sciences, School of Environmental Sciences, University of Liverpool, Liverpool, UK.
3. Research School of Earth Sciences, Australian National University, Canberra, ACT 2601, Australia

Accepted for publication by *Nature Geoscience*

Author Accepted Manuscript

Resubmitted on 14 December 2017

Restricting global warming to remain below agreed targets requires limiting carbon emissions, the principal driver of anthropogenic warming. However, there is significant uncertainty in projecting the amount of carbon that can be emitted, in part due to the limited number of Earth system model simulations and their discrepancies with present-day observations. Here, we demonstrate a novel approach to reduce the uncertainty of climate projections; using theory and geological evidence we generate a very large ensemble (3×10^4) of projections that closely match records for nine key climate metrics, including warming and ocean heat content. Our analysis narrows the uncertainty in surface warming projections and reduces the range in equilibrium climate sensitivity. We find that a warming target of 1.5°C above the preindustrial requires the total emitted carbon from the start of year 2017 to be less than 195 to 205 PgC (in over 66% of simulations), while a warming target of 2 °C is only likely if the emitted carbon remains less than 395 to 455 PgC. At current emission rates, these warming targets are reached in 17 to 18 years and 35 to 41 years, respectively, so that there is a limited window to develop a more carbon-efficient future.

The Paris Climate Agreement[1] aspires to restrict the rise in global-mean surface temperature since preindustrial times to 2 °C or less for this century by reducing global carbon emissions, the principal driver of anthropogenic warming[2]. However, there are large uncertainties in how much carbon may be emitted before meeting a warming target[3]. For example, a subset of 13 Earth system models[4,5] (from the Climate Model Intercomparison Project phase 5; CMIP5) suggests that 2 °C warming may be met by cumulative carbon emissions ranging from 84 to 581 PgC from year 2017 following Representative Concentration Pathway (RCP)[6] 8.5 (Fig. 1a; Supplementary Table 1). A large ensemble of simple climate model simulations[7] obtain an even wider uncertainty range for the maximum permitted cumulative carbon emission to avoid 1.5 ^{o}C warming, ranging from at least 250 to 540 PgC from year 2015 in 33% of their simulations (and extending even further from less than 200 to more than 850 PgC in 66% of their simulations). Clearly, the large uncertainties in permitted future carbon budget to meet specific warming targets need to be reduced.

In our view, a significant part of the large uncertainties in how much carbon may be emitted is due to discrepancies between model simulations and historical data. CMIP5 models are powerful tools to explore warming projections, solving for the climate response to radiative forcing and providing

emergent properties, such as the equilibrium climate sensitivity. However, there are mismatches between the CMIP5 simulations and historical reconstructions; for example, model projections of surface temperature differ from historical records[8-12] (Figs. 1b & 2a, grey band) with an average model-data mismatch of 0.2 °C (for the time-averaged temperature anomaly from the late-nineteenth century time-average and the period 1986 to 2005), and several models have too high a global ocean heat content from year 1980 onward compared with observational reconstructions[13-18] (Fig. 1c). Such discrepancies with observation-based reconstructions introduce uncertainty into future warming projections, which could be biased towards either too much or too little warming.

Generating observationally-constrained warming projections

Here, we present a complementary approach to make 21st century projections of surface warming projections, which is designed to minimise the model-data mismatch for the historical record. We exploit our theory for how warming connects to carbon emissions[19,20] to drive an efficient Earth system model (the Warming, Acidification and Sea-level Projector[21,22], Methods). Using geological evidence[23] for the equilibrium climate sensitivity, we produce an ensemble of climate simulations that spans the uncertainty in observational reconstructions of warming[8-12], ocean heat uptake[13-18] and carbon fluxes[2,24]. Our approach is similar to the 'history matching' approach applied to statistical emulators of complex Earth system models[25,26], except that here we use an efficient mechanistic Earth system model in place of a statistical emulator.

Our theory[19,20] demonstrates how the global-mean surface temperature anomaly relative to the preindustrial at time t, $\Delta T(t)$, is related to cumulative carbon emissions, $I_{em}(t)$ (in PgC), and the weighted sum[27-29] of radiative forcing from all forcing agents since preindustrial times, $\Delta R_{total}^{weighted}(t)$ (in Wm^{-2}), modified by the planetary heat uptake and the changes in ocean and terrestrial carbon inventories,

$$\Delta T(t) = \frac{aS}{I_B}\left(1-\frac{\varepsilon_N N(t)}{\Delta R_{total}^{weighted}(t)}\right)\left(\frac{\Delta R_{total}^{weighted}(t)}{\Delta R_{CO2}(t)}\right)\left(I_{em}(t)+I_{Usat}(t)-\Delta I_{ter}(t)\right), \qquad (1)$$

where a=5.35±0.27 Wm^{-2} is the CO_2-radiative forcing coefficient[2], S (in K $[Wm^{-2}]^{-1}$) is an empirically-determined[30] climate sensitivity, $N(t)$ (in Wm^{-2}) is the planetary heat uptake and effectively represents ocean heat uptake, $\Delta R_{CO2}(t)$ (in Wm^{-2}) is the radiative forcing from CO_2, ε_N is a non-dimensional weighting (referred to as the efficacy) for ocean heat uptake[30], I_{Usat} (in PgC) is

the global ocean undersaturation of dissolved inorganic carbon[19] with respect to instantaneous atmospheric CO_2, ΔI_{ter} (in PgC) is the cumulative change in residual terrestrial carbon storage since the preindustrial, and I_B (in PgC) is the preindustrial buffered carbon inventory of the global atmosphere and ocean system[19] of around 3500 PgC. The climate sensitivity, S, is related to the equilibrium climate sensitivity, ΔT_{2xCO2}, defining the surface air temperature change for a sustained doubling of atmospheric CO_2, by $S=\Delta T_{2xCO2}/(a \ln 2)$. In eq. (1), the efficacy of ocean heat uptake, ε_N, accounts for how the heat uptake $N(t)$ may have a different impact upon $\Delta T(t)$ than an equivalent radiative forcing from CO_2, $\Delta R_{CO2}(t)$ (Ref. 30), while radiative forcing from aerosols and non-well mixed greenhouses gases may be weighted[27-29] (with an efficacy, ε_i, differing from 1), such that $\Delta R_{total}^{weighted}(t) = \Delta R_{CO2}(t) + \sum \varepsilon_i \Delta R_i(t)$, where i sums over all other forcing agents, ε_i=1 for well mixed greenhouse gases and ε_i is referred to as ε_{aero} for aerosols.

Our efficient Earth system model[21,22] exploits our surface warming relationship (1) to make climate simulations from the preindustrial and projections for the 21st century. The model assumes that the empirical parameters a, S, I_B, and the non-dimensional weightings ε_N and ε_i, are constant with time, and then applies these parameters within an 8-box representation of the atmosphere-ocean-terrestrial system (see Ref. 21, Fig. 2 therein: Methods). The model solves, with time, for the global surface temperature anomaly, $\Delta T(t)$, planetary heat uptake, $N(t)$, carbon emissions, $I_{em}(t)$, ocean carbon undersaturation, $I_{Usat}(t)$, and residual terrestrial carbon storage, $\Delta I_{ter}(t)$, for prescribed CO_2 and radiative forcing pathways[21,22] (Methods, eqn. 1).

First, we use our efficient Earth system model to generate 10^8 simulations integrated from years 1765 to 2016, where each simulation has a unique set of 18 model parameter values that are varied independently between the simulations (Methods; Supplementary Table 2). The prior choices of the climate sensitivity, S, and resulting equilibrium climate sensitivity, ΔT_{2xCO2}, are taken from a frequency-density distribution of a geological reconstruction for the Cenozoic[23] (~the last 65 Ma), with S ranging from 0.48 to 1.96 K $(Wm^{-2})^{-1}$ and ΔT_{2xCO2} from 1.8 to 7.3 °C at 95% bounds (Fig. 3, black full lines). This initial set of 10^8 simulations is then tested for consistency against observations (Supplementary Table 3), using 9 observational constraints of historic warming[8-12], ocean heat content[13-18] (Supplementary Table 4) and carbon flux reconstructions[2,24]. Only 3×10^4 simulations (0.03%) pass the full consistency test, and then form our 'realistic ensemble' of simulations that are consistent with historical records (Supplementary Table 3) and within

uncertainty bounds for ocean heat uptake (Fig. 1c,d), surface warming (Figs. 1 and 2a, black line), and ocean and terrestrial carbon uptake (Supplementary Fig. 1).

Second, the 3×10^4 observation-consistent configurations of our efficient Earth system model are integrated forward from the start of year 2017 to 2100 for atmospheric CO_2, following standard RCP scenarios and including forcing of non-CO_2 greenhouse gases and aerosols[6] (Methods; Supplementary Table 3), while retaining the historic uncertainty in radiative forcing from different sources (Supplementary Fig. 2).

Observationally-consistent pathways towards warming targets

The observation-consistent simulations reach a surface temperature anomaly of 2 °C above the late nineteenth century average between years 2040 and 2052 for RCP8.5 (Fig. 2d, 95% confidence bands). Regarding other pathways, 2 °C warming is only slightly delayed to between years 2045 and 2076 for RCP4.5 (Fig. 2c), while most simulations (93%) remain under 2 °C warming by year 2100 for RCP2.6 (Fig. 2b). In comparison, the IPCC AR5 Earth system model ensemble suggests that 2 °C warming occurs within a much wider window between years 2026 to 2063 for RCP8.5; in addition, 22% of the AR5 models suggest that RCP4.5 might be sufficient to remain below a 2 °C warming target through the 21st century (compared to less than 1% of simulations for our observation-consistent ensemble).

Next, we assess the statistical likelihood of restricting surface warming to a maximum of 1.5 or 2.0 °C, in terms of the additional cumulative carbon emitted from the start of year 2017 (Fig. 4). For a given future cumulative carbon emission, our ensemble projections indicate that warming is 'likely' to be below a given target if at least 66% of simulations agree (adopting AR5 terminology[2]). Surface warming of 1.5 °C remains likely until cumulative carbon emissions reach between 195 and 205 PgC from the start of year 2017 (Fig. 4a,b; Table 1). Surface warming of 2.0 °C or less remains likely until the cumulative carbon emission reaches 395 to 455 PgC from the start of year 2017 (Fig. 4a,c; Table 1). By the time cumulative carbon emissions reach 540 PgC since year 2017, more than 75% of the projections have warming of 2.0 °C or more for both RCP8.5 and RCP4.5. Assuming our current carbon emission rate[24], the 1.5 °C warming target is likely to occur in 17 to 18 years and the 2 °C warming target is likely to be reached in 35 to 41 years. In comparison, by only allowing observation-consistent ensemble simulations, our range for the maximum permitted carbon emission for a 1.5 °C target is more restrictive than a recent large ensemble of climate

model simulations[7], which instead suggested a higher possible permitted cumulative carbon emission of at least 250 to 540 PgC from year 2015.

Reducing uncertainty in climate sensitivity and future warming

Our observationally-consistent projections of future surface temperature anomaly make different underlying assumptions than are made for complex Earth system models[2,5], and so the two approaches are complementary.

The CMIP5-based projections[2,5], based upon complex Earth system models, solve for the climate response and their emergent properties include climate sensitivity[31-35] and the non-dimensional weightings of radiative forcings[27-29] and heat imbalances[30,36], ε_i and ε_N (eqn. 1). Inter-model differences[37] in their projections arise from differences in their emergent equilibrium climate sensitivity, and in how each model takes up heat and carbon, and non-CO_2 radiative forcing. However, there are differences between the CMIP5-based projections over the historical record and the observations (Fig. 1b,c).

In contrast, our projections are designed to lie within the uncertainty bounds of the historical observations, including for warming and heat uptake. However, our projections require prior input distributions for model parameters, including climate sensitivity and the non-dimensional efficacy weightings, ε_I and ε_N, which are then held constant in time.

We now perform a set of perturbation experiments to test the robustness of our results with respect to the prior distributions of model parameters in the initial 10^8 simulations, (Supplementary Table 5, Methods). These perturbation experiments use 6 alternative input distributions for model parameters, including an alternative geological distribution[23] for climate sensitivity, S (Fig. 3, black dotted lines), and alternative distributions for the efficacy of heat uptake, ε_N, the efficacy of aerosol radiative forcing, $\varepsilon_{\text{aero}}$, and the uncertainty in the radiative forcing from aerosols. These perturbation experiments support our inferences for projected warming from the default experiment (Fig. 4, compare grey and blue lines; Supplementary Table 6). Across all perturbation experiments for RCP8.5, the maximum cumulative emission at which 66% of simulations remain under a warming target of 1.5 °C only varied between 195 and 205 PgC and under a warming target of 2 °C only varied between 395 and 405 PgC from the start of year 2017 (Table 1).

Within our ensemble of observation-consistent simulations, both the variation in warming projections and posterior equilibrium climate sensitivity are correlated to the simulated values of multiple historical constraints (Methods: Supplementary Fig. 4; Supplementary Table 8): warming projections are most correlated to historic simulated temperature change (R^2=0.2), but are also correlated to simulated historic ocean heat uptake (R^2=0.13); while the equilibrium climate sensitivity is most correlated to ocean heat uptake (R^2=0.3) and then historic temperature change (R^2=0.08). Thus, for the model projections to have any skill, reconstructions of both historic surface temperature and ocean heat uptake are needed (Fig. 1b,c).

Climate sensitivity is a key model parameter in determining the projected warming within our ensemble (Methods: Supplementary Table 9). An improved posterior estimate of the climate sensitivity is obtained from our two-stage process of assuming a prior estimate from geological reconstructions and then updating by the observational-consistent simulations (Fig. 3). This posterior estimate of equilibrium climate sensitivity lies between 2.0 to 4.3 °C based upon 95 % of the observation-consistent ensemble of simulations (Fig. 3, blue and grey lines; Supplementary Table 7). This posterior estimate is narrower than either of the prior distributions from geological evidence[23] (Fig. 3 black solid and dotted lines), and does not support the lowest values (from 1.5 to 2.0 ^{o}C) of the AR5 likely range[2] for equilibrium climate sensitivity of 1.5 to 4.5 °C. This narrowing of the geological estimate[23] for climate sensitivity (Fig. 3) is interpreted as the historical constraints revealing the part of the climate sensitivity range for the entire Cenozoic[23] that is applicable for the present day.

Implications for the Paris Agreement

The Paris Agreement[1] aims to keep the global surface temperature anomaly within 2.0 °C of preindustrial, and preferably close to 1.5 °C. Our analysis, using an observation-consistent ensemble of projections from an efficient Earth system model, is consistent with the observed trend between additional warming and cumulative emissions continuing into the future (Fig. 4a), and with previous studies that identified a near-linear link between warming and cumulative emissions[38-40, 19] (Fig. 4a). Our projections suggest that a likely chance of meeting the 1.5 °C warming target requires that cumulative carbon emissions remain below 195 to 205 PgC from the start of 2017, while a 2 ^{o}C warming target requires that cumulative carbon emissions remain below 395 to 455 PgC. The 1.5 and 2 °C warming targets are reached in 17 to 18 years and in 35 to 41 years, respectively, if the carbon emission rate is assumed to remain at its present-day value. Hence,

immediate action is required to develop a carbon-neutral or carbon-negative future[41,42] or, alternatively, prepare adaptation strategies for the effects of a warmer climate.

Acknowledgements

We acknowledge the World Climate Research Programme's Working Group on Coupled Modelling, which is responsible for CMIP, and we thank the climate modelling groups (listed in Supplementary Table 1 of this paper) for producing and making available their model output. For CMIP the U.S. Department of Energy's Program for Climate Model Diagnosis and Intercomparison provides coordinating support and led development of software infrastructure in partnership with the Global Organization for Earth System Science Portals. This work was supported by UK NERC grants NE/P01495X/1 and NE/N009789/1. GLF acknowledges support from UK NERC grants NE/D00876X/2, NE/I005595/1 and NE/P011381/1. EJR acknowledges Australian Laureate Fellowship FL120100050.

Author contributions

PG and RGW led the writing of the manuscript, with contributions from all co-authors. PG conducted the numerical experiments, which were conceived by PG and GLF. EJR provided the geological climate sensitivity distribution. VMR analysed the CMIP5 Earth system model output. AK and RGW analysed the ocean heat re-analysis records.

References

1. UNFCCC. *Adoption of the Paris Agreement*. Report No. FCCC/CP/2015/L.9/Rev.1, http://unfccc.int/resource/docs/2015/cop21/eng/l09r01.pdf (UNFCCC, 2015)
2. IPCC (2013) Climate Change 2013: The Physical Science Basis, CUP.
3. Meinshausen, M., *et al*., Greenhouse-gas emission targets for limiting global warming to 2°C. *Nature*, 458, 1158–1162, (2009).
4. Jones C., *et al.,* Twenty-First-Century Compatible CO_2 Emissions and Airborne Fraction Simulated by CMIP5 Earth System Models under Four Representative Concentration Pathways. *J. Climate*, 26, 4398-4413, (2013).
5. Collins M *et al.,* Long-term Climate Change: Projections, Commitments and Irreversibility. In: Climate Change 2013: The Physical Science Basis. Contribution of Working Group I to the Fifth Assessment Report of the Intergovernmental Panel on Climate Change [Stocker, TF et al. (eds.)]. Cambridge University Press, Cambridge, UK and New York, USA, (2013).
6. Meinshausen M., *et al*., The RCP greenhouse gas concentrations and their extensions from 1765 to 2300. *Clim. Change,* 109, 213–241, doi:10.1007/s10584-011-0156-z, (2011).
7. Millar R.J., *et al*., Emission budgets and pathways consistent with limiting warming to 1.5ºC. Nature Geoscience, doi:10.1038/NGEO3031, (2017).
8. Morice, C. P., J. J. Kennedy, N. A. Rayner & P. D. Jones, Quantifying uncertainties in global and regional temperature change using an ensemble of observational estimates: the HadCRUT4 dataset, *J. Geophys. Res.*, 117, D08101, doi:10.1029/2011JD017187, (2012). Dataset accessed 2017-01-19 at https://crudata.uea.ac.uk/cru/data/temperature/
9. GISTEMP Team: *GISS Surface Temperature Analysis (GISTEMP)*. NASA Goddard Institute for Space Studies, (2017). Dataset accessed 2017-01-19 at https://data.giss.nasa.gov/gistemp/.
10. Hansen J., S. Ruedy, M. Sato & K. Lo, Global surface temperature change*, Rev. Geophys.*, 48, RG4004, (2010).
11. Smith T. M., R. W. Reynolds, T. C. Peterson & J. Lawrimore, Improvements to NOAA's historical merged land–ocean surface temperature analysis (1880–2006), *J. Clim.*, 21, 2283–2296, (2008).
12. Vose R. S., *et al.,* NOAA's merged land-ocean surface temperature analysis. *Bulletin Amer. Meteorol. Soc.*, 93, 1677–1685, doi:10.1175/BAMS-D-11-00241.1, (2012).
13. Levitus, S., et al., World ocean heat content and thermosteric sea level change (0–2000 m), 1955–2010, *Geophys. Res. Lett.* 39.10, (2012).
14. Giese, B.S., & S. Ray, El Niño variability in simple ocean data assimilation (SODA), 1871–2008, *J. Geophys. Res.: Oceans,* 116.C2, (2011).
15. Balmaseda, M. A., K. Mogensen & A. T. Weaver, Evaluation of the ECMWF ocean reanalysis system ORAS4, *Quart. J. Roy. Met. Soc.* 139.674,1132-1161, (2013).
16. Good, S.A., M.J. Martin & N.A. Rayner, EN4: Quality controlled ocean temperature and salinity profiles and monthly objective analyses with uncertainty estimates, *J. Geophys. Res. Oceans,* 118.12, 6704-6716, (2013).
17. Smith, D.M., *et al.* Earth's energy imbalance since 1960 in observations and CMIP5 models. *Geophys. Res. Let.,* 42.4: 1205-1213, (2015).
18. Cheng, L., *et al.*, Improved estimates of ocean heat content from 1960 to 2015. *Science Advances,* 3.3, e1601545, (2017).
19. Goodwin, P., R. G. Williams & A. Ridgwell, Sensitivity of climate to cumulative carbon emissions due to compensation of ocean heat and carbon uptake. *Nature Geosci.*, 8, 29–34, (2015).
20. Williams, R. G., P. Goodwin, V. M. Roussenov & L. Bopp, A framework to understand the Transient Climate Response to Emissions. *Environmental Research Letters*, 11, doi:10.1088/1748-9326/11/1/015003, (2016).
21. Goodwin P., How historic simulation–observation discrepancy affects future warming projections in a very large model ensemble, *Clim. Dyn*., 47, 2219–2233, doi: 10.1007/s00382-015-2960-z, (2016).
22. Goodwin, P., I. D. Haigh, E. J. Rohling & A. Slangen, A new approach to projecting 21st century sea-level changes and extremes, *Earth's Future*, 5, 240–253, doi:10.1002/2016EF000508, (2017).
23. Rohling, E. J., *et al*, Making sense of palaeoclimate sensitivity, *Nature* 491, 683-691, doi:10.1038/nature11574, (2012).
24. le Quéré, C., *et al.,* Global Carbon Budget 2016. *Earth Syst. Sci. Data*, 8, 605–649, doi:10.5194/essd-8-605-2016, (2016).

25. Williamson, D., M. Goldstein, L. Allison, A. Blaker, P. Challenor, L. Jackson & K. Yamazaki L., History matching for exploring and reducing climate model parameter space using observations and a large perturbed physics ensemble, *Clim. Dyn.,* 41, 1703-1729, doi:10.1007/s00382-013-1896-4, (2013).
26. Williamson, D., A.T. Blaker, C. Hampton & J. Salter, Identifying and removing structural biases in climate models with history matching, *Clim. Dyn.,* 45, 1299, doi:10.1007/s00382-014-2378-z, (2015).
27. Marvel, K., G. A. Schmidt, R. L. Miller and L. S. Nazarenko, Implications for climate sensitivity from the response to individual forcings, *Nature Climate Change*, 6, p386-389, doi: 10.1038/NCLIMATE2888, (2015).
28. Shindell, D. T., Inhomogeneous forcing and transient climate sensitivity, *Nature Climate Change*, 4, p274-277, doi: 10.1038/NCLIMATE2136, (2014).
29. Hansen, J., et al.,. Efficacy of climate forcings. *Journal of Geophysical Research: Atmospheres*, 110 (D18), doi:10.1029/2005JD005776, d18104, (2005)
30. Winton, M., Takahashi K. & I. Held, Importance of ocean heat uptake efficacy to transient climate change, *J. Climate,* 23, 2333-2344, (2010).
31. Armour, K. C., Bitz, C. M. & Roe, G. H. Time-varying climate sensitivity from regional feedbacks. *J. Clim.* **26**, 4518–4534, (2013).
32. Gregory, J. M., and T. Andrews, Variation in climate sensitivity and feedback parameters during the historical period, *Geophys. Res. Lett.,* 43, 3911—3920, doi:10.1002/2016GL068406, (2016).
33. Armour, K. C., Energy budget constraints on climate sensitivity in light of inconstant climate feedbacks, *Nature Climate Change*, 7, p331-335, doi: 10.1038/NCLIMATE3278, (2017).
34. Rugenstein, M. A. A., K. Caldeira, and R. Knutti, Dependence of global radiative feedbacks on evolving patterns of surface heat fluxes, *Geophys. Res. Lett.,* 43, 9877–9885, doi:10.1002/2016GL070907, (2016).
35. Knutti, R. & G. C. Hergerl, The equilibrium sensitivity of the Earth's temperature to radiation changes, *Nature Geoscience* 1, 735-743, doi:10.1038/ngeo337, (2008).
36. Geoffroy, O. *et al.,* Transient climate response in a two-layer energy-balance model. Part II: representation of the efficacy of deep-ocean heat uptake and validation for CMIP5 AOGCMs. *J Clim* 26, 1859–187, DOI: 10.1175/JCLI-D-12-00196.1, (2013)
37. Williams, R.G., V. Roussenov, P. Goodwin, L. Resplandy & L. Bopp, Sensitivity of global warming to carbon emissions: effects of heat and carbon uptake in a suite of Earth system models. *J. Climate*, doi: 10.1175/JCLI-D-16-0468.1, (2017).
38. Allen, M. R., Frame, D. J., Huntingford, C., Jones, C.D., Lowe, J. A., Meinshausen, M. & Meinshausen, N., Warming caused by cumulative carbon emissions towards the trillionth tonne. *Nature* 458, 1163-1166, (2009).
39. Matthews, H. D., Gillet, N. P., Stott, P. A. & Zickfield, K., The proportionality of global warming to cumulative carbon emissions. *Nature* 459, 829-832, (2009).
40. Gillet, N. P., Arora, V. K., Matthews, D. & Allen, M. R., Constraining the ratio of global warming to cumulative CO_2 emissions using CMIP5 simulations. *J. Climate* 26, 6844-6858, (2013).
41. Rogelj, J., *et al.*, Paris Agreement climate proposals need a boost to keep warming well below 2C. *Nature* 534.7609, 631-639, (2016).
42. Rockström, J., *et al*., A roadmap for rapid decarbonisation, *Science,* 24, 355, 6331, 1269-1271. doi: 10.1126/science.aah3443, (2017).

Figure Captions and Tables

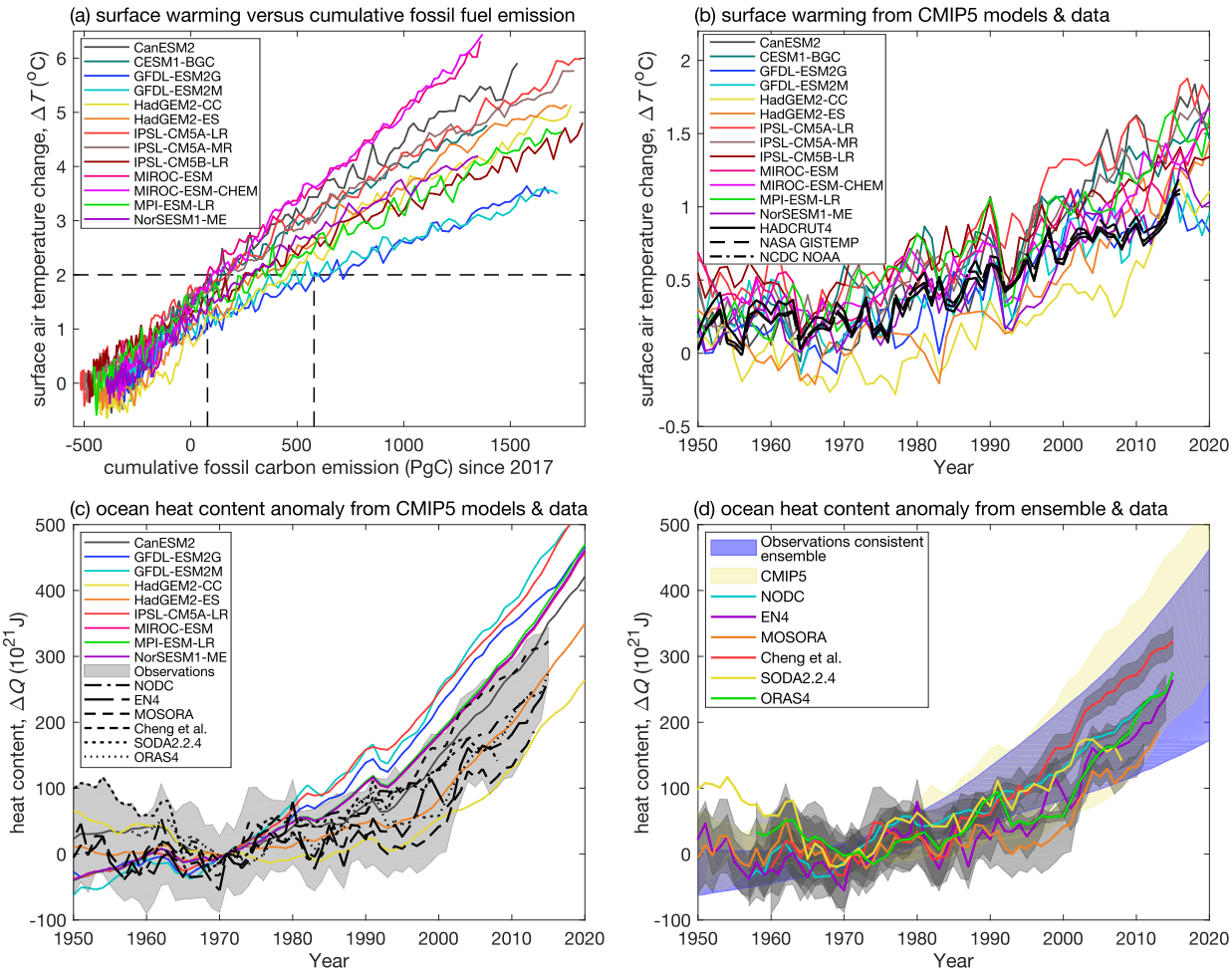

Figure 1. Surface warming projections and ocean heat content anomalies. (a) Global surface air temperature anomaly (°C) from 13 Earth system models relative to the late-nineteenth century time-average (Methods) from year 1861 to 2100 following RCP8.5 (lines) versus cumulative fossil-fuel carbon emissions (PgC) since year 2017. The grey dashed lines indicate when the projected warming exceeds 2 °C in cumulative fossil-fuel emission. (b) Global surface air temperature anomaly (°C) relative to the late nineteenth century time-average (Methods) with time from three different data-based reconstructions and 13 Earth system models from year 1950 to 2016 (observations) and to 2020 (models) following RCP8.5 (lines) (c) Historical reanalyses for global ocean heat content, ΔQ (10^{21}J) over the full depth, relative to 1971 from available observational analyses and reanalysis products, together with 9 different CMIP5 model variants (lines). (d) ΔQ (10^{21}J) over the full depth, relative to 1971 for 9 different CMIP5 Earth system models (yellow shading) and the observation-consistent ensemble of our conceptual Earth system model simulations (blue shaded) with projections up to year 2020; note ΔQ for NODC and Cheng et al. are for 0-2000 m depth while others are full-depth. The grey shaded areas show the uncertainty for the heat content anomalies.

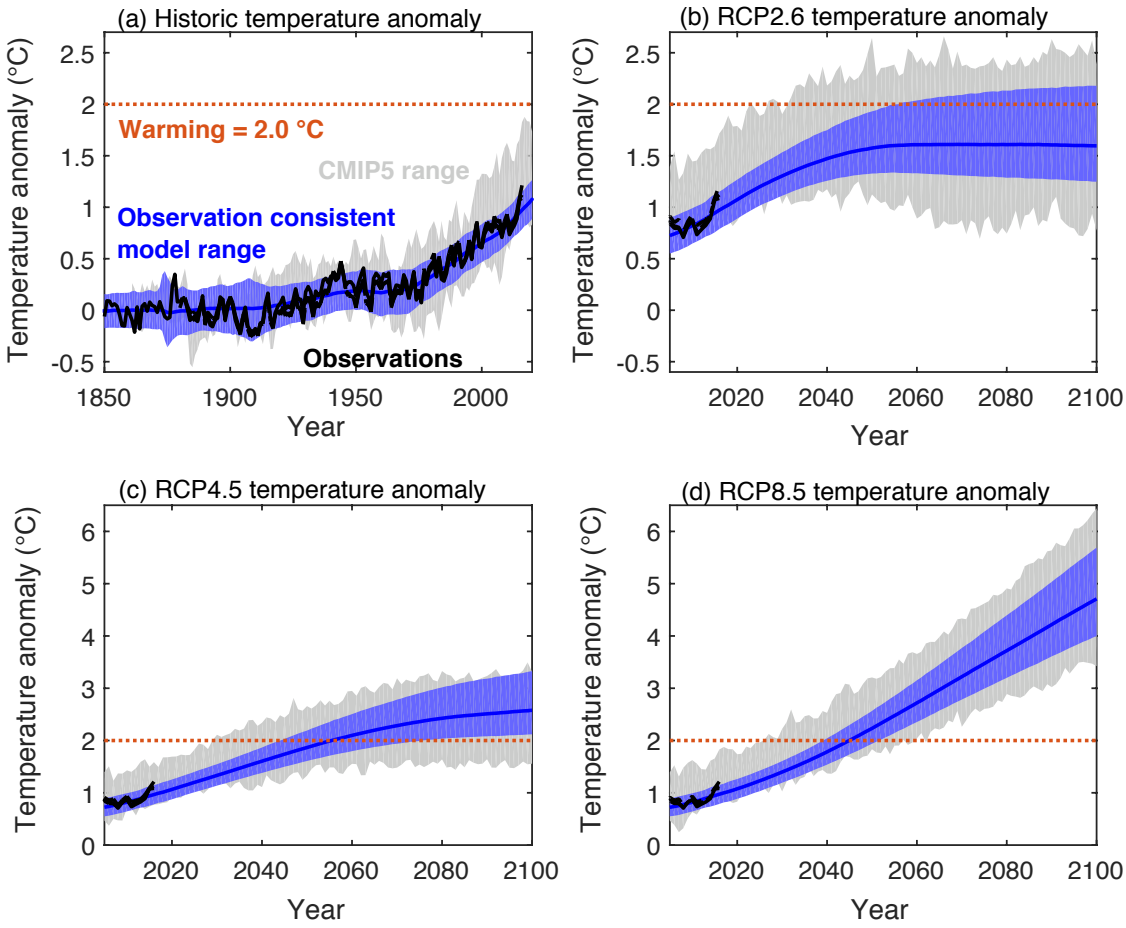

Figure 2. Global mean surface temperature anomaly over time from observations and model simulations. The temperature anomaly relative to the late nineteenth century time-average for three observational records (black lines as in Fig. 1b), the range of selected CMIP5 Earth system models (grey shaded area) and the observation-consistent ensemble from our efficient Earth system model (blue shaded area is 95% range; blue line is median) from: (a) year 1861 to 2020, and year 2005 to 2100 for (b) RCP2.6, (c) RCP4.5 and (d) RCP8.5. Note that the model simulations in panel (a) employ the high-end, RCP8.5, scenario to extend to year 2020.

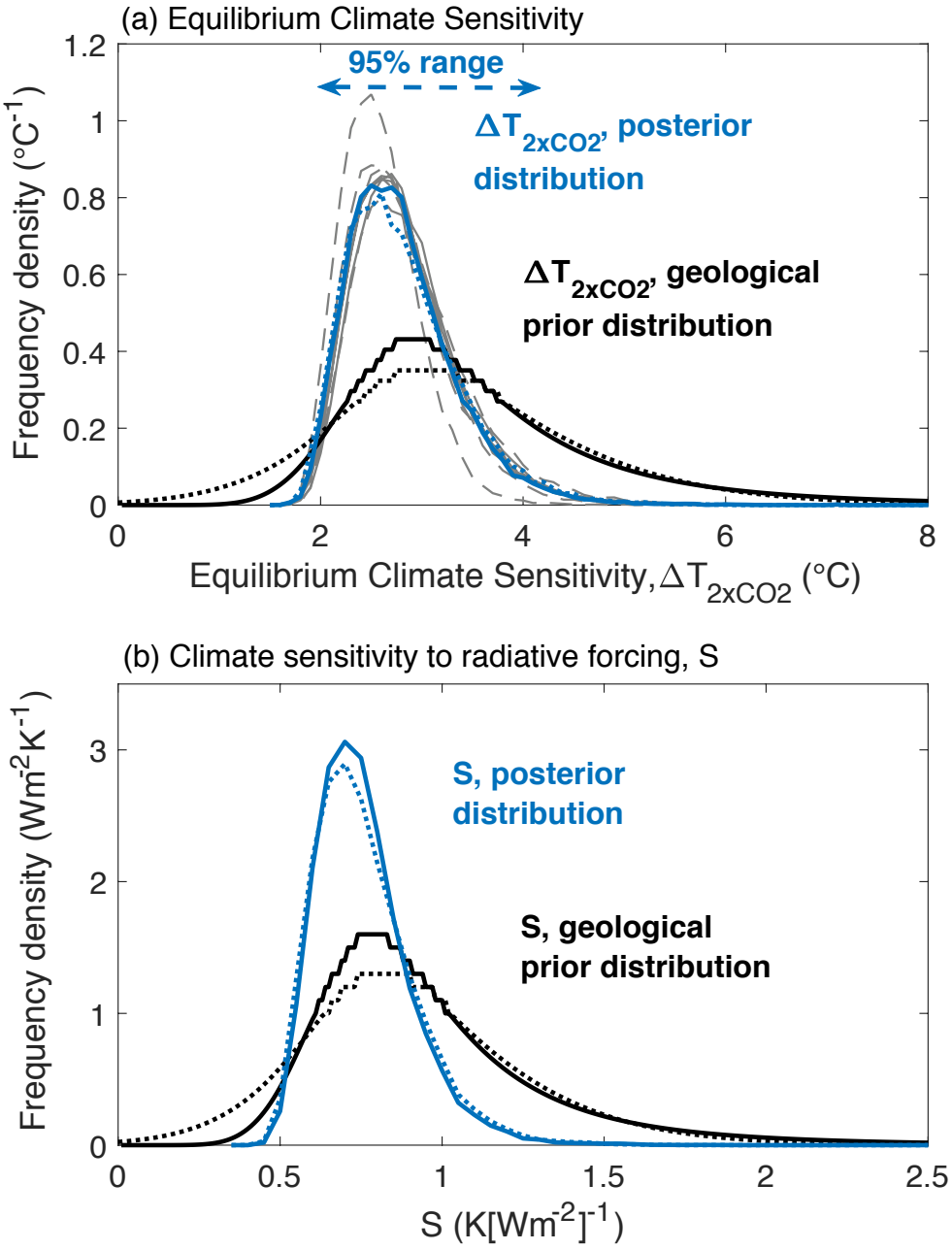

Fig. 3: Model ensemble parameter distributions for (a) equilibrium climate sensitivity and (b) climate sensitivity. Input distributions in the initial 10^8 efficient Earth system model simulations (black) and the final distribution in the 10^4 observation-consistent simulations for RCP8.5 (blue). The climate sensitivity parameter, *S*, where the input distribution is taken from geological evidence (black solid line) and for the final geologically and observationally-constrained ensemble (blue solid line). The different distributions are included for the alternative geological reconstruction input distribution (black dotted line) and resulting alternative observationally-constrained ensemble (blue dotted line) and the observation-constrained ensembles for the other RCP scenarios (grey solid lines) and the perturbation experiments for RCP8.5 (grey dashed lines) (Supplementary Table 5).

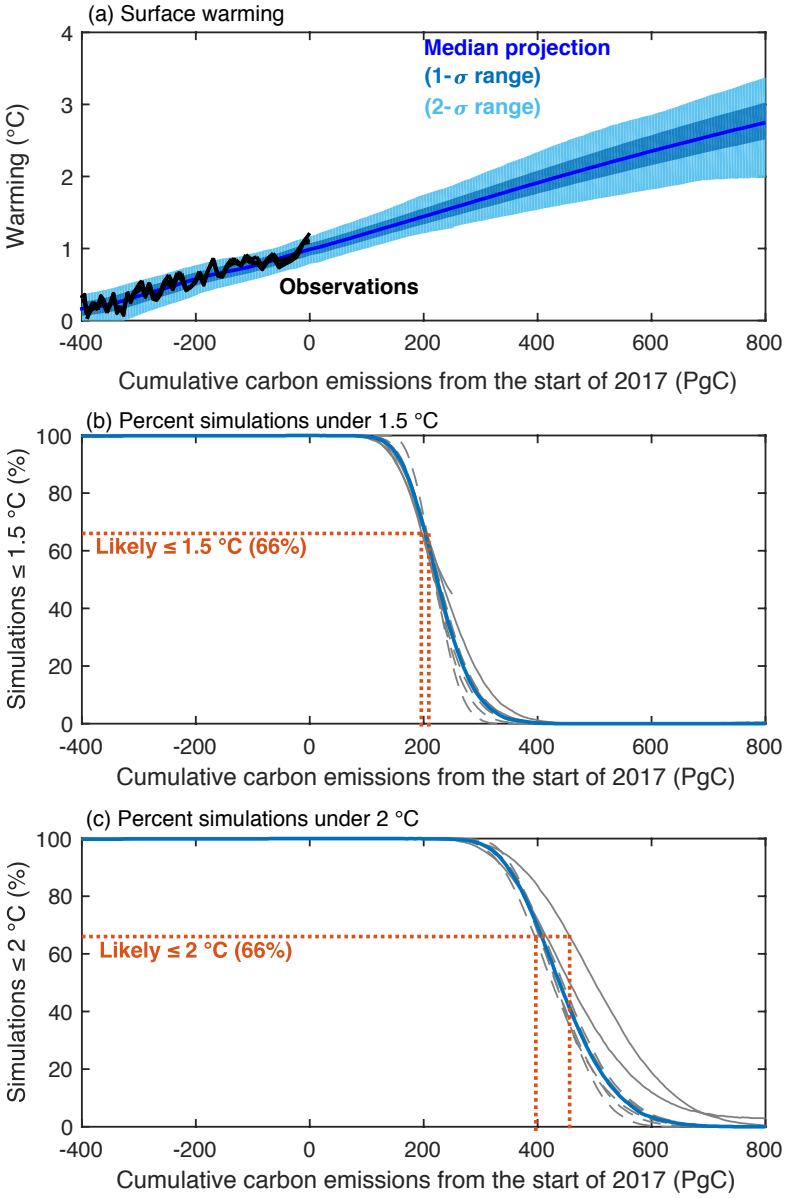

Figure 4. Cumulative carbon emissions and warming projections from our observationally-consistent ensemble. (a) Global-mean surface temperature anomaly relative to the year 1850-1900 average against cumulative carbon emitted since the start of year 2017. Shown are the observation-consistent ensemble (blue line and dark blue shaded area are the median and 66% range for the RCP8.5 standard experiment, light blue is the 95% range across all RCP scenarios for the standard experimental configuration: Methods) and observations (black lines as in Fig. 1b). For the observational reconstructions (black lines), cumulative carbon emissions prior to year 2017 are calculated from the Global Carbon Project reconstructions (Ref. 24) and warming is from the three reconstructions as in Fig. 1b. The percentage of observationally-constrained simulations that remain with warming of (b) 1.5 °C or under and (c) 2 °C or under, relative to the year 1850-1900 average against additional carbon emitted since the start of year 2017 (Solid blue line is the RCP8.5 standard experiment, grey solid lines are the standard experiments with alternative RCP scenarios, and grey dashed lines are for alternative input distribution experiments: Methods).

Experiment	Max emissions for warming ≤ 1.5 °C in 66 % of simulations	Max emissions for warming ≤ 1.5 °C in 50 % simulations (5 to 95 %)	Max emissions for warming ≤ 2 °C in 66 % of simulations	Max emissions for warming ≤ 2 °C in 50 % of simulations (5 to 95 %)
1. Standard experiment	200 PgC	220 PgC (145 to 315)	405 PgC	435 PgC (320 to 580)
2. Perturbation experiments for RCP8.5	195 to 205 PgC	215 to 225 PgC (135 to 325)	395 to 410 PgC	425 to 440 PgC (315 to 590)

Table 1: Cumulative emissions from year 2017 when the 1.5 and 2 °C warming targets are exceeded for the standard modelling experiment and perturbation experiments, including different choices of climate sensitivity, S, ε_N, $\varepsilon_{\text{aero}}$ and aerosol radiative forcing (full details in Supplementary Tables 5 and 6). All non-standard experiments follow RCP8.5.

Methods

The displayed CMIP5 Earth system model output

A range of Earth system CMIP5 model results are displayed in Figures 1, 2 and 4 and Supplementary Fig. 1, and are taken from the Earth system models in Supplementary Table 1 (Refs. 43-51). Figure 1a and Figure 4a contain all 13 Earth system models. Figure 1b, Figure 2 and Figure 4b each contain 9 of the Earth system models: CanESM2, GFDL-ESM2G, GFDL-ESM2M, HadGEM2-CC, HadGEM2-ES, IPSL0CM5A-LR, MIROC-ESM, MPI-ESM-LR, NorESM1-ME. Figure 3c contains 8 of these Earth system models, excluding HadGEM2-CC.

The efficient Earth System Model

For our efficient Earth system model, we use the Warming Acidification and Sea level Projector (WASP) of Refs. (21,22). This model is integrated 100-million times with alternative parameter combinations to find simulations that agree with historic observational constraints (Supplementary Table 2). As configured in Refs. 21 and 22, WASP lacks stochastic behaviour in the global surface temperature anomaly. However, the observational constraints for surface warming (Supplementary Table 3) represent both the underlying trends and internal stochastic variability in the climate system. Therefore, model simulations that accurately represent the underlying trends in historic surface warming but lack stochastic behaviour still may not be consistent with the observational constraints. In order to maximise the possibility of including model simulations that both accurately represent the underlying trends in surface warming and agree with observations, we employ an additional stochastic surface temperature anomaly in WASP, applied to global mean surface air temperature, T, and global mean sea surface temperature, SST.

Since global temperature anomaly records are generally presented with 1-month resolution (Refs. 8-12), we employ a monthly time-step in WASP (altered from 10-per year in Refs. 21,22). A stochastic temperature anomaly, $T_{stochastic}$ (in °C), is then inserted to surface air temperatures and sea surface temperatures using a noise distribution (AR(2) noise),

$$T_{stochastic}(t) = c_1 T_{stochastic}(t-\delta t) + c_2 T_{stochastic}(t-2\delta t) + c_3 z_i(t), \qquad \text{(eq. 2)}$$

where δt is the 1-month model time step, c_1, c_2 and c_3 are non-dimensional tuned constants and z_i is a randomly assigned temperature anomaly between -1.0 and 1.0 K. The coefficients c_1, c_2 and c_3 are

tuned such that the simulated monthly global surface temperature anomaly has similar amplitude and autocorrelation properties to the monthly GISTEMP record between year 1971 and 2016. This is assessed by removing the linear trend in the NASA GISTEMP (Ref. 9) monthly record from year 1971 to 2016 to reveal the autocorrelation properties and the amplitude, with the variability having a root mean square of 0.14 °C. For comparison, the first 20 simulations accepted into the standard experiment observation consistent ensemble using RCP8.5 considered from year 1971 to 2016. With the linear trends in warming removed, the 20 simulations have an average root mean square amplitude variability of 0.13 °C, with a standard deviation of 0.04 °C between simulations, when using coefficient values are tuned to c_1=0.3, c_2=0.4 and c_3=0.062. These root mean square amplitude variability values of the 20 simulations are similar to the 0.14 °C value for the GISTEMP observations, and the simulations display similar autocorrelation properties.

Generating the observation-consistent model ensembles

A total of 10 model ensembles are constructed, each containing ~3×10^4 observation-consistent simulations. These 10 model ensembles comprise 4 ensembles using a standard experimental set up for each of four forcing scenarios, RCP8.5, RCP6.0, RCP4.5 and RCP2.6, and a further 6 ensembles using alternative experimental set ups all following RCP8.5 scenario.

First, an initial prior ensemble[21] of 10^8 model configurations is constructed by independently varying 18 model parameters with specified prior distributions (Supplementary Table 2 for experiment 1, and see Supplementary Table 3 for how this configuration is changed for the other experiments;). These model 18 varied model parameters represent the physical, chemical and biological properties of our efficient Earth system model. Each model configuration is then forced with historic CO_2 and radiative forcing followed by RCP scenarios from Ref. (6). In each of the initial 10^8 simulations the three raditvie forcing terms, from CO_2, other Kyoto agents (comprising well mixed greenhouse gasses other than CO_2 and CFCs) and non-Kyoto agents (principally aerosols) respectively (see Ref. 6), are independently varied with normal distributions, such that the distributions in year 2011 approximate the uncertainty in the three radiative forcing terms as assessed in Ref. (2) (Supplementary Table 2). The radiative forcing from well-mixed greenhouse gases other than CO_2 and aerosols (and non-Kyoto agents) are both varied using scaling coefficients that apply over all time to each property respectively (Supplementary Fig. 2). The input distribution for the initial 10^8 simulations for the climate sensitivity, S, is drawn from a probability distribution for the value of S in palaeoclimates assessed from a review of geological evidence over the Cenozoic (Ref. 23), using the distribution with log-normal uncertainty (Fig. 3, black solid lines).

At the end of year 2016, each of the 10^8 simulations are assessed using an observational-consistency test[21,22] that covers 9 observational constraints for surface warming[8-12, 52,53], ocean heat uptake[13-18,54-57] and carbon cycle fluxes[2,58-60] (Supplementary Table 4). A simulation passes the observation-consistency test if either all 9 simulated properties lie within the observed ranges (Supplementary Table 3), or if the total fractional sum of discrepancies from the observational ranges, δ_{error}, is less than 0.1. The fractional sum of discrepancies term, δ_{error}, is calculated from a summation over all observational constraints for which the simulated value lies outside the observational range (Supplementary Table 4) using,

$$\delta_{error} = \sum \left(\frac{|x_i - y_i|}{\Delta_{yi}} - 1 \right), \qquad \text{(eq. 3)}$$

where x_i is the simulated model value, y_i is the mid-point of the observational constraint range, Δ_{yi} is the observation-consistent range in the observational constraint (i.e. from the minimum to maximum value in Supplementary Table 4) and δ_{error} is summed only over those i constraints for which x_i lies outside the observational consistent region, $y_i \pm 0.5\Delta_{yi}$. This inclusion of simulations in the final posterior distribution provided $\delta_{error}<0.1$ (eq. 3) allows some tolerance for simulations to be considered observation-consistent, removing potential bias that might arise from applying artificially narrow observational constraints when selecting the final model ensemble.

In the standard experiment, the prior input distribution for the efficacy of heat uptake ε_N is normal, with mean and standard deviation from the distribution of 16 CMIP5 models analysed by Ref. (36) (Supplementary Table 2, Supplementary Figure 3), while the prior input distribution for efficacy of aerosol radiative forcing ε_{aero} is uniform, ranging from 0.33 to 3.0 (Supplementary Table 2, Supplementary Fig. 4). Although note that the posterior distribution of ε_{aero} sees values concentrated towards 1, while the posterior distribution of ε_N stays close to the prior input distribution from CMIP5 models (Supplementary Figure 3).

Perturbation experiments are conducted with different input parameter distributions (Supplementary Table 5). For all experiments except experiment 7, only 0.03 % of the initial ensemble simulations pass the observation-consistency test, producing a final observation-consistent ensemble of 3×10^4 simulations. This observation-consistent ensemble displays good agreement with the full ranges for

all the observational quantities (Supplementary Table 4), demonstrating that the 3×10^4 simulations have good coverage of observational parameter space. For experiment 7, 0.08 % of the initial ensemble pass the observation-consistency test, thus requiring only 4×10^7 initial simulations to produce ~3×10^4 observation-consistent simulations. This is because any given simulation is more likely to be observation-consistent when ε_{aero}=1 (Supplementary Figure 3, notice peak value in the posterior distribution of ε_{aero} in the standard experiment).

Generating the observational consistency test

The observational constraint ranges follow the 90 to 95% confidence for each property and where a single constraint is based on multiple records, the allowable range is widened to encompass the confidence ranges of each observational record. The nine observational constraints in the observational consistency test are listed in Supplementary Table 3. The ocean heat uptake constraints are based on the observational records in Supplementary Table 4. To generate the limits of the ocean heat uptake constraints, we consider the range from the minimum to maximum of the individual observation reconstructions, including the 2-sigma uncertainty (Fig. 1c,d).

The surface air-temperature constraint from years 1850-1900 to 2003-2012 is the estimated 90% confidence range from AR5 (Ref. 2). The surface air-temperature constraints from years 1951-1960 to 2007-2016 and 1971-1980 to 2007-2016 are based on the HadCRUT4, GIST EMP and NCDC records (Refs. 8-12). The 2-sigma error in the decadal temperatures from the HadCRUT4 record is estimated at ±0.05 °C from 1950 to the present (Ref. 8), while the 2-sigma error in the annual GISTEMP record is also estimated at ±0.05 °C (Ref. 10). Therefore, we estimate a 95% confidence range in the surface air-temperature constraints from 1951-1960 to 2007-2016 and from 1971-1980 to 2007-2016 by allowing an additional ±0.05 °C relative to the minimum and maximum of the HadCRUT4, GISTEMP and NCDC records, noting that the HadCRUT4 and GISTEMP records represent the minimum and maximum values for both constraints respectively.

The sea surface temperature constraint from years 1850-1900 to 2003-2012 is based on the average of the HadSST3 (accessed from https://crudata.uea.ac.uk/cru/data/temperature/ on 2017-01-19: Ref. 53) and NCDC ERSST (accessed from https://www.ncdc.noaa.gov/monitoring-references/faq/anomalies.php on 2017-01-19: Ref. 53) records, but with ±0.06 K uncertainty to mimic the 90% confidence uncertainty in global surface air-temperatures over the same period from AR5. The ocean and terrestrial carbon uptake constraints derive from AR5 assessments (Ref. 2).

Calculation of global surface temperature anomalies

The Earth system model temperature anomalies are calculated relative to the 1861-1900 period. The observational temperature anomalies are calculated relative 1850-1900 for the HadCRUT4 record, and relative to 1880-1900 for the NCDC and GISTEMP records (which begin in 1880). For the efficient Earth system model, the surface temperature anomaly is calculated relative to the simulated 1850-1900 time-average separately in each simulation, except for Supplementary Table 8 and Supplementary Figure 4 where the temperature anomaly is calculated relative the preindustrial steady state of the model before radiative forcing is imposed.

Code availability: The computer code for our efficient Earth system model, the Warming Acidification and Sea-level Projector, is available within the supplementary material for this manuscript.

Data availability: Data that supports this study has been deposited in British Oceanographic Data Centre published data library database (dataset title: "Observation consistent warming projections for 2081-2100 from the WASP model for the RCP4.5 scenario, and the corresponding earth system properties", by Goodwin, P. et al.). All other data supporting this study is available within the supplementary material of this manuscript.

Additional references from Methods and Supplementary Information:

43. Arora, V. K. *et al.,* Carbon emission limits required to satisfy future representative concentration pathways of greenhouse gases. *Geophysical Research Letters*, 38 (5), L05 805, doi:10.1029/ 2010GL046270, (2011).

44. Moore, J., K. Lindsay, S. Doney, M. Long, and K. Misumi, Marine Ecosystem Dynamics and Biogeochemical Cycling in the Community Earth System Model [CESM1(BGC)]: Comparison of the 1990s with the 2090s under the RCP4.5 and RCP8.5 Scenarios. *J. Climate,* **26**, 9291–9312, doi: 10.1175/JCLI-D-12-00566.1, (2013).

572
573 45. Dunne, J. P. *et al.*, GFDLs ESM2 Global Coupled Climate Carbon Earth System Models. Part II: Carbon
574 System Formulation and Baseline Simulation Characteristics. *Journal of Climate*, 26 (7), 2247–2267,
575 doi:10.1175/JCLI-D-12-00150.1, (2013).

576 46. Martin, G. M. *et al.*, The HadGEM2 family of Met Office Unified Model climate configurations. *Geosci.*
577 *Model Dev.*, 4 (3), 723–757, doi:10.5194/gmd-4-723-2011, (2011).

578 47. Jones, C. D. *et al.*, The HadGEM2-ES implementation of CMIP5 centennial simulations. *Geosci. Model*
579 *Dev.*, 4 (3), 543– 570, doi:10.5194/gmd-4-543-2011, (2011).

580 48. Dufresne, J.L. *et al.,* Climate change projections using the IPSL-CM5 Earth System Model:
581 from CMIP3 to CMIP5. *Climate Dynamics*, 40, 2123-2165, (2013).
582
583 49. Watanabe, S., *et al.*, MIROC-ESM 2010: model de- scription and basic results of CMIP5-20c3m
584 experiments. *Geosci. Model Dev*, 4, 845–872, doi:10.5194/gmdd-4-1063-2011, (2011).
585
586 50. Giorgetta, M. A. *et al.*, Climate and carbon cycle changes from 1850 to 2100 in MPI-ESM simulations
587 for the Coupled Model Intercomparison Project phase 5: Climate Changes in MPI-ESM. *Journal of*
588 *Advances in Modeling Earth Systems*, 5 (3), 572–597, doi:10.1002/jame.20038, (2013).

589 51. Tjiputra, J. F. *et al.*, Evaluation of the carbon cycle components in the Norwegian Earth System Model
590 (NorESM). *Geosci. Model Dev.*, 6 (2), 301–325, doi:10.5194/ gmd-6-301-2013, (2013)

591 52. Kennedy, J.J., Rayner, N.A., Smith, R.O., Saunby, M. and Parker, D.E., Reassessing biases and other
592 uncertainties in sea-surface temperature observations measured in situ since 1850 part 2: biases and
593 homogenisation. *Journal of Geophysical Research* 116, D14104, doi:10.1029/2010JD015220, (2011)
594
595 53. Huang, B., V.F. Banzon, E. Freeman, J. Lawrimore, W. Liu, T.C. Peterson, T.M. Smith, P.W. Thorne,
596 S.D. Woodruff, and H. Zhang, Extended Reconstructed Sea Surface Temperature Version 4 (ERSST.v4).
597 Part I: Upgrades and Intercomparisons. *J. Climate*, 28, 911–930, doi: 10.1175/JCLI-D-14-00006.1, (2015).
598
599 54. Domingues, C. M., *et al*., Improved estimates of upper-ocean warming and multi-decadal
600 sea-level rise. *Nature,* **453**, 1090-1093, (2008).
601
602 55. Ishii, M., & M. Kimoto, Reevaluation of historical ocean heat content variations with an XBT
603 depth bias correction. *J. Oceanogr*., **65**, 287-299, doi:10.1007/s10872-009-0027-7, (2009).
604

605 56. Smith, D. M. & J. M. Murphy, An objective ocean temperature and salinity analysis using covariances
606 from a global climate model. *J. Geophys. Res.*, **112**, C02022, doi:10.1029/2005JC003172, (2007).
607
608 57. Carton, J. A. & B. S. Giese, A Reanalysis of Ocean Climate Using Simple Ocean Data Assimilation
609 (SODA). *Mon. Weather Rev*., **136**, 2999-3017, (2008).
610
611 58. Boden, T.A., G. Marland, and R.J. Andres. Global, Regional, and National Fossil-Fuel CO2 Emissions.
612 Carbon Dioxide Information Analysis Center, Oak Ridge National Laboratory, U.S. Department of Energy,
613 Oak Ridge, Tenn., U.S.A. doi 10.3334/CDIAC/00001_V2016, (2016).
614
615 59. Houghton, RA, van der Werf, GR, DeFries, RS, Hansen, MC, House, JI, Le Quéré, C, Pongratz, J and
616 Ramankutty, N. Chapter G2 Carbon emissions from land use and land-cover change, *Biogeosciences*, 9,
617 5125-514, (2012).
618
619 60. Khatiwala, S, Tanhua, T, Mikaloff Fletcher, SE, Gerber, M, Doney, SC, Graven, HD, Gruber, N,
620 McKinley, GA, Murata, A, Rios, AF and Sabine, CL. Global ocean storage of anthropogenic carbon,
621 *Biogeosciences*, 10, 2169-2191, (2013).
622